

# An Overview of the Formation and Attitude Control System for the Terrestrial Planet Finder Interferometer

Daniel P. Scharf,\* Fred Y. Hadaegh, Zahidul H. Rahman,  
Joel F. Shields, Gurkupal Singh, and Matthew R. Wette

*Jet Propulsion Laboratory, California Institute of Technology,  
4800 Oak Grove Dr., Pasadena, CA 91109-8099 USA*

The Terrestrial Planet Finder formation flying Interferometer (TPF-I) will be a five-spacecraft, precision formation operating near the second Sun-Earth Lagrange point. As part of technology development for TPF-I, a formation and attitude control system (FACS) is being developed that achieves the precision and functionality needed for the TPF-I formation and that will be demonstrated in a distributed, real-time simulation environment. In this paper we present an overview of FACS and discuss in detail its formation estimation, guidance and control architectures and algorithms. Since FACS is currently being integrated into a high-fidelity simulation environment, component simulations demonstrating algorithm performance are presented.

## I. Introduction

NASA's Terrestrial Planet Finder (TPF) mission will search for Earth-like planets orbiting other stars and probe their atmospheres for indications of life.<sup>1,2</sup> ESA's Darwin mission has similar goals.<sup>3</sup> TPF has baselined two architectures: an optical-wavelength coronagraph (TPF-C), and an infrared formation flying interferometer (TPF-I). For TPF-I observations, inter-spacecraft ranges and bearings must be maintained to 2 cm and 1 arcmin, respectively, and attitudes must be maintained to within 1 arcmin. Hence, TPF-I is a precision formation. These performance requirements are derived from (i) the instrument requirement that the optical path difference between the arms of the interferometer be on the order of a nanometer (for nulling in the near-infrared) and (ii) system-level trades regarding active optics and optical delay lines.

To mitigate mission risk and advance formation flying technology, the TPF project has been developing several formation flying testbeds. In particular, the Formation Algorithms and Simulation Testbed (FAST) is a distributed real-time simulation environment that will demonstrate end-to-end operation of a formation flying mission with TPF-level functionality and precision. FAST will address formation complexity issues such as formation time synchronization, inter-spacecraft communication with latencies, inter-spacecraft sensing and data fusion, and system-wide formation robustness. Additionally, FAST is responsible for developing a Formation and Attitude Control System (FACS) for demonstrating end-to-end precision formation flying operation of a preliminary TPF-I design. The specific hardware architecture, flight-like software executive, distributed simulation architecture, and initial results of FAST are described in Ref. 5.

Formation control requires both traditional attitude control systems (ACS) and relative translational control systems. These two control systems are generally coupled. For example, estimating a relative spacecraft position requires the attitudes of two spacecraft. Combined attitude and relative translational control systems are referred to as a Formation and Attitude Control System (FACS).

This paper provides an overview of the formation and attitude control system being developed for TPF-I technology demonstration. Specifically, we discuss the architectures and algorithms used for precision formation estimation, guidance and control of TPF-I, as well as the spacecraft dynamic models used for algorithm

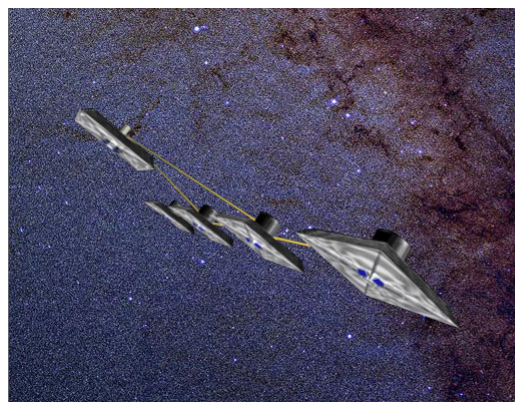


Figure 1. TPF Formation Flying Interferometer.

\*Corresponding Author. Email: Daniel.P.Scharf@jpl.nasa.gov, Phone:(818)-354-4795, Fax: (818)-393-0342

development and validation. In addition, we present preliminary performance results for these algorithms, which are currently being integrated into FAST’s end-to-end, distributed real-time simulation environment. The performance of the formation in this high-fidelity simulation environment will be the subject of a future paper.

The remainder of this paper is organized as follows. First, we introduce the baseline TPF-I spacecraft design used for FACS development. Then the overall architecture of FACS is discussed. Next, we present the architectures and specific algorithm designs for formation estimation, guidance and control. We also include performance results based on stand-alone, component simulations in Simulink. Finally, we present some conclusions.

## II. Baseline TPF-I Spacecraft Design for FACS Development

The TPF-I flight design is still evolving. However, a fixed baseline design was created for FACS development. As the flight design continues to evolve, updates are integrated into the FACS baseline design consistent with the scope of the TPF-I formation flying testbeds. Moreover, FACS is being designed to be adaptable to a number of flight designs. For example, the formation control architecture will function with spacecraft in a line or at the corners of a square.

The baseline design has the characteristics of the flight design important for FACS design. For example, the current sun-shield design is square while the FACS baseline sun-shield is round, but the salient feature of the sun-shield is retained, namely, a fundamental mode of approximately 0.5 Hz. In the following we only present the details of the baseline spacecraft design relevant to FACS design, namely, mass and dynamic properties, actuators, sensors and inter-spacecraft communication.

The TPF-I formation consists of four collectors and one combiner. The collectors are equally-spaced along a line. The combiner forms an isosceles triangle with the two inner collectors. Spacecraft sun-shield separations range from 5 to 100 m. See Figures 1 and 2. Until a more mature combiner design is available, we use five collectors for FACS design. The collector model is shown in Figure 3. The addition of a combiner will necessitate minor retuning of the FACS control and estimation algorithms, but no structural changes. The baseline collector design is shown in Figure 3. Mass and dynamic properties are given in Table 1.

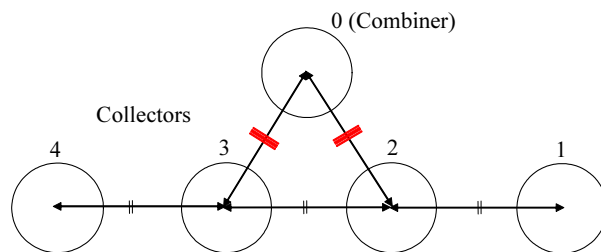


Figure 2. TPF-I Science Configuration.

Table 1. Baseline Design Mass & Dynamic Properties.

Property	Value
Mass	879 kg
$I_{xx}$	2787 kg m <sup>2</sup>
$I_{yy}$	2836 kg m <sup>2</sup>
$I_{zz}$	2266 kg m <sup>2</sup>
Off-Diagonal Inertias	< 1.5% of $I_{xx}$
First Structural Mode	0.48 Hz

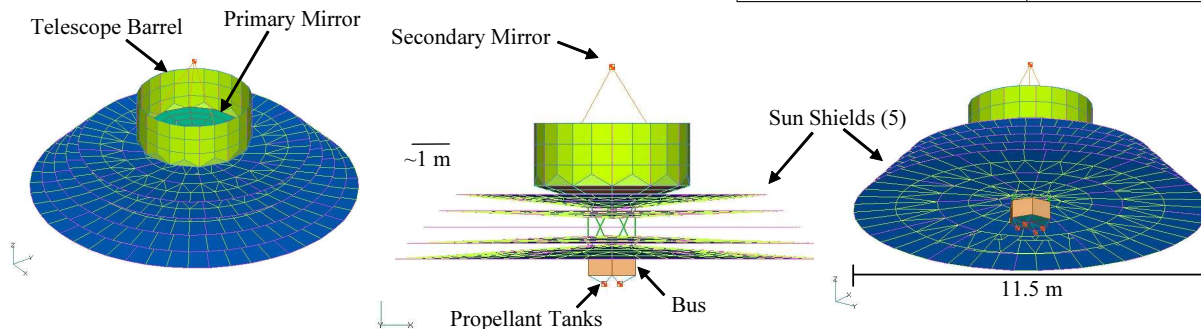


Figure 3. Baseline Collector Design for FACS Development.

## A. Actuators

Each spacecraft has 6-DOF uncoupled control authority via pulse-width modulated (i.e., constant force) thrusters. Reaction wheels are also available for attitude control. The thrusters are assumed to be configured to provide a minimum translational impulse of  $0.5 \text{ mN s}$  and a minimum rotational impulse of  $0.15 \text{ mN m s}$ . The reaction wheels will be sized when the sun-shield design and observation maneuvers (e.g., formation rotation period) are finalized.

## B. Sensors

For attitude estimation, each spacecraft is equipped with sun sensors, a gyro and two star-trackers. The second star-tracker reduces the measurement uncertainty about the boresight of the first. For relative translational estimation, each spacecraft has an accelerometer, and three relative sensing suites: acquisition, medium and fine. The medium and fine sensors have conical fields-of-view. The capabilities of each suite are given in Table 2.

**Table 2. Relative Sensor Properties**

Sensor	Range <i>km</i>	FOV <i>deg.</i>	Range Acc. <i>cm</i> $1\sigma$	Bearing Acc. <i>arcmin</i> $1\sigma$
Acquisition	10	Full Sky	50	60
Medium	0.1	10	1	1
Fine	0.1	10	0.1	0.067

Each relative sensing suite has a different sensing topology. The acquisition sensor has a  $4\pi$  steradian field-of-view (FOV): each spacecraft can measure the position of every other spacecraft that is in range, barring occultations. The medium and fine sensors have limited fields-of-view. Their sensing topologies are shown in Figures 4 and 5, respectively. Note that measurements are made on specific spacecraft as indicated by the solid circles in the figure. Considering the fine sensing topology, no single spacecraft has the ability to make a precision estimate of the entire formation without communication.

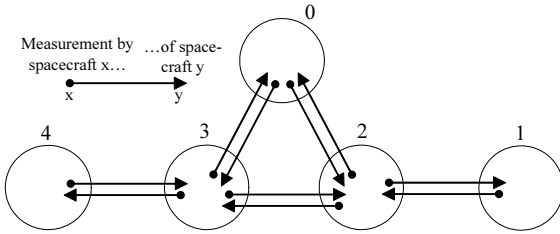


**Figure 4. Medium Relative Sensor Topology.**

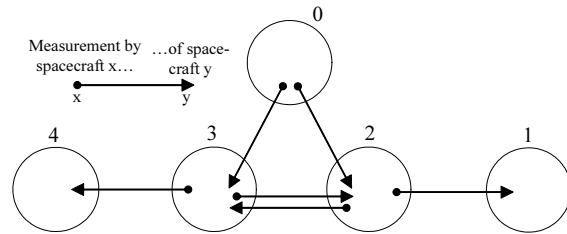


**Figure 5. Fine Relative Sensor Topology.**

## C. Inter-Spacecraft Communication

Each spacecraft can communicate with every other spacecraft. The current flight design is to route communication through the combiner. For nominal FACS design, however, the exact topology is not important as long as bandwidth is sufficient. For design, bandwidth is assumed sufficient for FACS needs.

During initialization of the formation, spacecraft clocks are synchronized to  $20 \text{ ms}$ . Due to the synchronization, it is possible to communicate FACS information in two windows. The communication windows are discussed in the next section. Assuming direct point-to-point communication and no margin, a preliminary estimate of the peak bandwidth needed by FACS in these windows is  $160 \text{ kbps}$ . Further optimization of data size (e.g., floats vs. doubles) will reduce this number. However, the driving requirements for inter-spacecraft communication are the inter-spacecraft pointing control loops for the interferometer's fast steering mirrors. These loops are sampled at  $1 \text{ kHz}$ . As a result, the current design of the TPF-I inter-spacecraft communication system supports  $2 \text{ Mbps}$ .

## III. Formation and Attitude Control System Overview

The FACS contains all the elements of a general control system: an estimator to determine the values of the controlled variables, a path planner (referred to as guidance) to determine the desired values for the controlled variables, and a controller to drive the difference between the estimated and desired values to zero.

In addition, a mode commander coordinates the different levels of functionality of the overall system. For example, guidance cannot begin to command a formation rotation until the estimator declares that relative position estimates are sufficiently accurate.

As much as possible, FACS software is identical on each spacecraft. However, as discussed in the following sections, the combiner serves as a leader for relative translational control and guidance. Additional functionality is activated aboard the combiner by designating in software the combiner as a leader and the collectors as followers. It is possible to specify one of the collectors as leader.

The FACS on each spacecraft runs at a rate of 1 Hz, resulting in a realtime interval (RTI) of 1 s. This period is adjustable within limits. The estimation and guidance architectures discussed in the following sections require inter-spacecraft communication (ISC). Figure 6 shows both how the RTI is divided on each spacecraft and when ISC occurs. The numbers in the figure represent a fraction of RTI. All local sensors and commands from guidance, ground and mode commander are read by 0.1 RTI. By 0.2 RTI the first part of FACS, referred to as FACS1, has run. FACS1 includes the mode commander and the attitude estimator. Then the local quaternion and other information needed for relative translation estimation are communicated between spacecraft in the first communication window from 0.2 RTI to 0.4 RTI. Between 0.4 RTI and 0.75 RTI, the second part of FACS runs. This FACS2 includes the relative translation estimator, the guidance and the attitude and relative translation controllers. Actuator commands are written to the actuator managers by 0.75 RTI. During the second communication window from 0.75 RTI to 1.0 RTI, mode commander and guidance information is communicated.

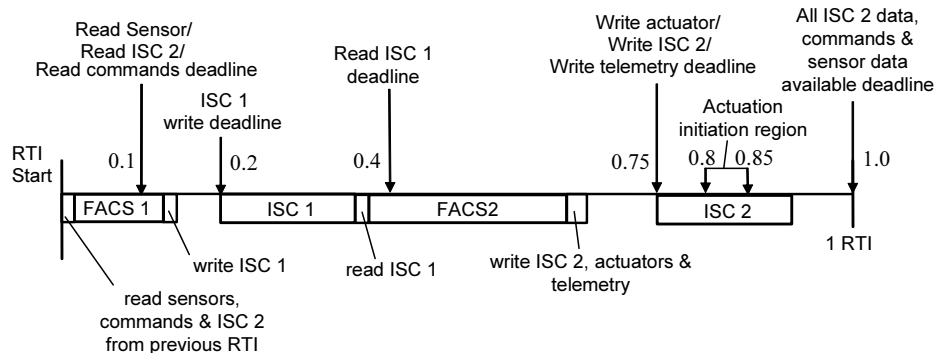


Figure 6. FACS Realtime Timing and Communication.

Finally, TPF-I performance requirements are the most stringent during scientific observations. The formation must be rotated as a virtual rigid body and relative range and bearing controlled to 2 *cm* and 1 *arcmin* respectively. Attitudes must be controlled to 1 *arcmin*. Since the sun-shields are 15.3 *m* in diameter, the 1 *arcmin* bearing requirement translates into a 6 *mm* position requirement at minimum 5 *m* spacecraft separations.

## IV. Formation and Attitude Estimation

### A. Estimation Architecture

The estimator must provide estimates of the controlled variables. As will be discussed in Section VI, each spacecraft must control its inertial attitude, and each collector must control the position of its center-of-mass (CM) with respect to the combiner’s CM. Each spacecraft estimates its own attitude independently using a gyro, star trackers and a Kalman filter.

In addition to the controlled relative position variable, we require each spacecraft to know the location of all the other spacecraft for collision avoidance. Furthermore, a centralized estimator that communicates this information to all spacecraft introduces a single point failure mode. Therefore, a decentralized relative translation estimation architecture is used for robustness. Each spacecraft estimates the positions of all other spacecraft CMs with respect to its own based on local measurements and on communicated measurements and data.

The communicated data includes quaternion estimates and CM acceleration estimates. The CM acceleration estimates are needed to propagate the relative translational equations of motion. The CM acceleration estimates are produced by an Acceleration Data Processing algorithm on each spacecraft discussed subse-

quently.

One complication in relative translational estimation is that it is coupled one way to attitude estimation. Relative sensors provide measurements between sensor frames on respective spacecraft. However, since a CM-to-CM relative position vector is desired for control, the estimator must transfer from the two sensor frames (one on each spacecraft involved in the measurement) to CM-located body frames. This transfer requires the attitudes of both spacecraft.

For measurement-based propagation, accelerometers and gyros are sampled at 10 Hz. The star trackers and relative sensors provide measurements at 1 Hz. Propagation occurs at a higher rate to more accurately determine thruster cut-off times. The 10 Hz accelerometer and gyro measurements are stored and then processed in batch during FACS1 (see Figure 6).

## B. Attitude Estimation Algorithm

The attitude estimator uses a Kalman filter that includes gyro bias states. Recall two star trackers are used. Star tracker measurement accuracies are  $3 \text{ arcsec } 1\sigma$  about the transverse axes and  $24 \text{ arcsec } 1\sigma$  about the boresight axis. Precision gyro specifications were used to demonstrate the algorithm: an angle random walk variance of  $5.3 \times 10^{-13} \text{ rad}^2/\text{s}^2$ , a rate random walk variance of  $8.2 \times 10^{-18} \text{ rad}^2/\text{s}^3$ , and a correlation time of  $100 \text{ s}$ . Misalignments between the gyro and star tracker frames and the body frame are assumed to be of  $10 \text{ arcsec}$  magnitude. The performance of the attitude estimator under these conditions is shown in Figure 7, which shows the difference between estimated and true angular positions about each body axis. The biases are due to the frame misalignments. Spacecraft attitudes are estimated to an average accuracy of  $5.9 \text{ arcsec } 1\sigma$ , which is sufficient for attitude control. Detrended, the average performance of the estimator is  $0.9 \text{ arcsec } 1\sigma$ .

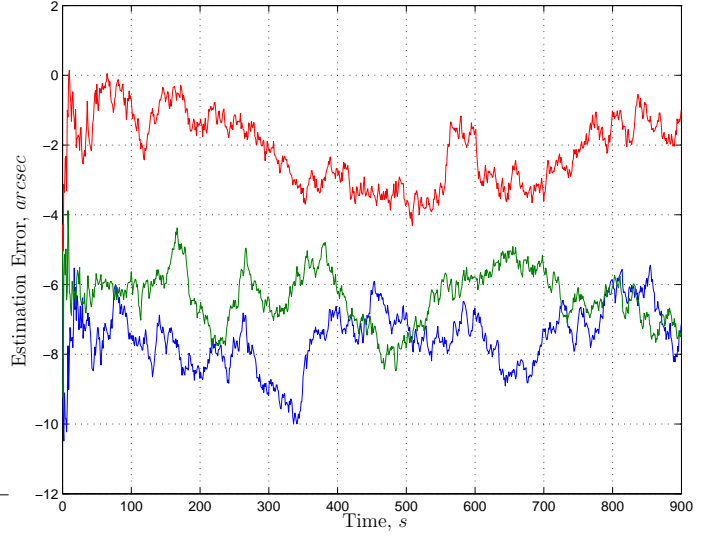


Figure 7. Attitude Estimation Error by Axis.

## C. Relative Translation Estimation Algorithm

The relative translational estimator has two components: a Kalman filter and an Acceleration Data Processing (ADP) algorithm, which produces bias-corrected CM acceleration estimates.

We consider the Kalman filter first. Since the spacecraft are in deep space, the relative translational dynamics are modelled by double integrators.<sup>6</sup> To illustrate the estimator design, Eqn. (1) is the propagation equation for spacecraft 4's estimator. The next two equations (2) and (3) are the measurement equations in terms of the state, which is used to design the Kalman filter, and in terms of the measured quantity, which is used to calculate the input to the estimator during operation. These two equations are for a medium sensor measurement between spacecraft 4 and 3 made on spacecraft 4. The state  $x$  is defined implicitly in (1):

$$\frac{d}{dt} \begin{bmatrix} x_{40}^I \\ x_{41}^I \\ x_{42}^I \\ x_{43}^I \\ \dot{x}_{40}^I \\ \dot{x}_{41}^I \\ \dot{x}_{42}^I \\ \dot{x}_{43}^I \end{bmatrix} = \begin{bmatrix} 0_{12 \times 12} & I_{12 \times 12} \\ 0_{12 \times 12} & 0_{12 \times 12} \end{bmatrix} \begin{bmatrix} x_{40}^I \\ x_{41}^I \\ x_{42}^I \\ x_{43}^I \\ \dot{x}_{40}^I \\ \dot{x}_{41}^I \\ \dot{x}_{42}^I \\ \dot{x}_{43}^I \end{bmatrix} + \begin{bmatrix} 0_{12 \times 12} \\ I_{12 \times 12} \end{bmatrix} \begin{bmatrix} a_0^I - a_4^I \\ a_1^I - a_4^I \\ a_2^I - a_4^I \\ a_3^I - a_4^I \end{bmatrix} + \begin{bmatrix} 0_{12 \times 12} \\ I_{12 \times 12} \end{bmatrix} \begin{bmatrix} w_{40} \\ w_{41} \\ w_{42} \\ w_{43} \end{bmatrix} \quad (1)$$

$$y = [0_{3 \times 3} \ 0_{3 \times 3} \ 0_{3 \times 3} \ C(q_{B^4}^{M^{43}})C(q_I^{B^4}) \ 0_{3 \times 12}]x + n_{43}^m \quad (2)$$

$$y_m = v_m + C(q_{B4}^{M43})r_{M43}^H - C(q_{B4}^{M43})C(q_I^{B4})C^T(q_I^{B3})r_{M43}^R \quad (3)$$

where the sensor measurement  $v_m$  is in the 4-to-3 medium relative sensor frame on spacecraft 4,  $x_{ij}^I$  is the position vector from spacecraft  $i$ 's CM to spacecraft  $j$ 's CM in the inertial frame,  $a_i^I$  is the inertial acceleration of spacecraft  $i$ 's CM in the inertial frame,  $w_{ij}$  is the process noise for spacecraft  $j$ 's CM position with respect to spacecraft  $i$ 's,  $n_{ij}^m$  is the sensor noise for the medium measurement from spacecraft  $i$  to  $j$ ,  $C(q)$  is the rotation matrix corresponding to quaternion  $q$ ,  $q_I^{Bi}$  is the quaternion from inertial frame to spacecraft  $i$ 's body frame,  $q_{B4}^{M43}$  is the quaternion from spacecraft 4's body frame to spacecraft 4's medium sensor frame for the measurement from 4 to 3,  $r_{M43}^H$  is the position of the relative sensor equipment needed for the medium measurement on the host spacecraft (i.e., spacecraft 4) in the host's body frame, and  $r_{M43}^R$  is the position of the relative sensor equipment needed for the medium measurement on the remote spacecraft (i.e., spacecraft 3) in the remote spacecraft's body frame.

Eqn. (3) illustrates the attitude coupling of the relative translation estimator. The quaternions  $q_I^{B4}$  and  $q_I^{B3}$  are provided by the attitude estimators on spacecraft 4 and 3, respectively. The quaternion  $q_I^{B3}$  must be communicated from spacecraft 3. Spacecraft 4 must also have a database containing the characteristics of spacecraft 3's sensor hardware. In the example above, a value for  $r_{M43p}^R$  must be stored. Similarly, to propagate the equations of motion (1) the accelerations  $a_i^I$ ,  $i = 0, 1, 2, 3$ , must be communicated among all spacecraft. Note that relative measurements in which spacecraft 4 is not involved are also included in the estimator. For example, a medium sensor measurement between spacecraft 2 and 0 can be represented using spacecraft 4's estimator state as  $x_{40}^I - x_{42}^I$ . In the case where the measurement is made on spacecraft 2, Eqn. (2) would be replaced by

$$y = [C(q_{B2}^{M20})C(q_I^{B2}) \ 0_{3 \times 3} \ -C(q_{B2}^{M20})C(q_I^{B2}) \ 0_{3 \times 3} \ 0_{3 \times 12}]x + n_{20}^m. \quad (4)$$

In Eqn. (1) the inertial CM accelerations  $a_i^I$  are calculated by the Acceleration Data Processing (ADP) algorithm aboard each spacecraft  $i$  and then communicated to all other spacecraft. The ADP consists of another Kalman filter for estimating the accelerometer bias, which is modelled as a constant term plus a random walk. The ADP also converts the acceleration measured by the accelerometer, which is not located at the CM, to the equivalent acceleration at the CM using gyro measurements. The quaternion estimate is used then to transform the acceleration from body frame to inertial frame.

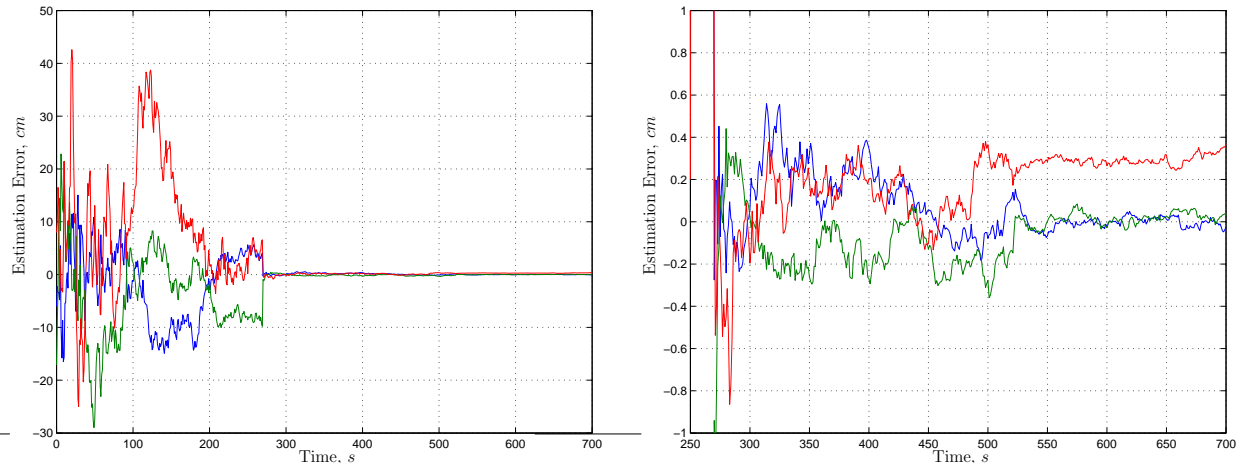
A challenge in relative translational propagation is that the thrusters are very small (e.g., 50  $mN$ ). As a result, for minimum on-time thruster firings the accelerometer signal-to-noise (SNR) can be very small. If the accelerometer measurement magnitude is below a threshold, then the ADP uses commanded thruster on-times to generate the effective acceleration via thruster models. This model-based acceleration approach provides more accurate acceleration estimates than low SNR accelerometer measurements.

Combining the ADP and the relative translational Kalman filter produces the full relative translational estimator. The performance of the estimator was demonstrated in a 700  $s$  simulation during which spacecraft 4 maneuvered to bring different relative sensors into lock. Figure 8 shows the estimation error of spacecraft 4's estimate of spacecraft 3's relative position. The simulation includes sensor-to-body frame misalignments of 10  $arcsec$  and sensor location uncertainties of 0.1  $mm$  (recall  $r_{M43}^H$  in (3)). The simulation includes the attitude estimator and attitude estimation errors. In Figure 8(a), the acquisition sensor is locked at the beginning. As can be seen, estimation errors are consistent with a 50  $cm$  measurement error (see Table 2). At 270  $s$ , the medium relative sensor locks, and the estimation error is reduced to less than 1  $cm$ . Figure 8(b) shows the performance during medium and fine lock with a finer ordinate scale. The fine sensor locks at 522  $s$ , and relative positions are then estimated to an average accuracy of 1.7  $mm \ 1\sigma$ . This level is sufficient for the 6  $mm$  control performance requirement. The biases apparent in Figure 8(b) are due to frame misalignments and sensor location uncertainties. Transforming to range and bearing based on the 50  $m$  spacecraft separation of this example, the average range estimation error is 0.13  $mm \ 1\sigma$  and the average bearing estimation error is 0.14  $arcmin \ 1\sigma$ .

## V. Formation and Attitude Guidance

### A. Guidance Architecture

The formation guidance provides reference trajectories to the relative translation and attitude controllers. As such, the output of the formation guidance depends on the particular control architecture. As discussed



(a) All Relative Sensing Stages: Acquisition Lock at 0 s, Medium Lock at 270 s, Fine Lock at 522 s. (b) Detail of Performance with Medium and Fine Relative Sensors.

**Figure 8. Relative Translation Estimation Error by Axis.**

subsequently in the Formation and Attitude Control section, attitudes are controlled independently and the relative positions are controlled via a Leader/Follower architecture. For attitude control, the formation guidance calculates desired quaternions, angular velocities and angular accelerations. For relative position control, the formation guidance calculates the desired position and velocity of each collector (follower) relative to the combiner (leader) and open-loop inertial acceleration profiles for all spacecraft.

For TPF-I there are three mission phases: Formation Acquisition, Formation Reconfiguration, and Observation. Formation acquisition, also known as formation initialization, is the process of obtaining relative dynamic state information and establishing communication. It occurs after deployment or a fault condition. Formation reconfiguration moves the formation from one configuration to a new configuration. Reconfigurations occur after acquisition to move the formation to its initial science configuration, and after a science observation to retarget. Finally, the observation phase consists of rotating the formation as a rigid body and changing its baseline (i.e., the distance between spacecraft 1 and 4 in Figure 2) to synthesize a synthetic aperture. The observation phase is unique in that spacecraft attitudes must be synchronized with relative positions for the interferometer to operate.

In each of these three phases formation guidance must command the formation, that is, provide attitude and relative translation paths for all the spacecraft.

A hybrid architecture was selected for the formation guidance. Relative translational paths are centrally planned on the combiner, while attitude planning is decentralized. Specifically, attitude paths are planned locally based on high-level commands from the combiner, for example, a final attitude and a final time. The relative translational guidance was centralized to ensure formation-wide constraint satisfaction and to reduce the complexity of synchronizing relative positions and attitudes during precision formation rotations.

In contrast to the estimation architecture, there is no robustness issue with centralized relative translational guidance. If a serious fault disables the combiner, all the spacecraft default to a stand-alone, safe stand-off mode where each spacecraft is responsible for its own collision avoidance. This stand-off mode is possible because the formation estimation is decentralized.

There are three main constraints that the attitude and relative translational paths must satisfy: the collision avoidance constraint (CAC), the sun avoidance constraint (SAC), and the relative thermal constraint (RTC). For the CAC, exclusion spheres are placed around each spacecraft, and relative translational paths must not cause the spheres to intersect. The SAC protects the infrared optics. It requires the payload “boresights” to remain within a cone about the anti-sun line. See Figure 9.

Finally, recall that TPF-I is an infrared interferometer. The optics are cooled to 40 K. The hot side of each spacecraft’s sun-shield is approximately 300 K. If the hot side of one spacecraft’s sun-shield were to illuminate the cold optics of another it would heat the optics. Then the formation would have to sit idle while the optics re-cool. For each spacecraft, the RTC requires that relative position vector to the other spacecraft remain approximately  $85^\circ$  or more away from the sun-shield normal. The RTC is a time-varying

attitude constraint that depends on the relative positions of the formation.

## B. Attitude Guidance Algorithm

The attitude guidance algorithms on each spacecraft are extensions of the attitude guidance algorithm designed for the Cassini mission.<sup>7</sup> On each spacecraft a base frame is defined by aligning (i) a body fixed direction with an inertial direction and (ii) a second body fixed direction as much as possible with a second inertial direction. Attitude turns are then commanded by specifying a new attitude relative to either the current or base frame.

When a new attitude is commanded, the guidance first checks if the new attitude violates the SAC. If it does, the command is rejected. If not, then an attitude path is first planned based on an Euler turn. If during this turn the SAC is violated, then the turn is broken into three Euler turns that do not violate the SAC. This algorithm does not address the RTC. However, the RTC is only active after the spacecraft are in science configuration. In science configuration attitude maneuvers are synchronized with relative positions so that the RTC is satisfied.

As an example of SAC satisfaction by the attitude guidance, consider Figure 9. The +Z body axis is the payload boresight of a collector. In this example, the boresight must remain within 30° of the anti-sun line, which is the +Z inertial axis. Per the guidance interface, this is equivalent to maintaining the angle  $\theta$  between the -Z inertial axis and the +Z body axis greater than 150°.

Figure 10 shows the guidance replanning to satisfy the SAC by plotting  $\theta$  versus time. First a rotation about the +X inertial axis places the boresight axis near the edge of the SAC cone. Then a 170° turn is commanded. If one Euler turn is used, the SAC is violated. However, the attitude guidance detects this violation and replans three smaller turns that all satisfy the SAC.

Recall that during the observation phase, attitudes must be synchronized with spacecraft relative positions. This synchronization is accomplished by continually specifying the second inertial direction of the base frame to be the rotating baseline direction. In this case, attitude and translational guidance is centralized, since the baseline direction is updated each RTI by the combiner. Alternatively, to maintain decentralized attitude guidance, the second inertial direction can be assigned to be the vector to a neighboring spacecraft. Then each spacecraft would estimate this vector and calculate attitude commands individually.

## C. Relative Translation Guidance Algorithms

We consider each of the three mission phases. For formation acquisition, recall that the acquisition sensor has an unlimited FOV. See Table 2. Further, the baseline TPF-I design includes omni-directional communication. As a result, formation acquisition consists of turning these systems on. If there is an acquisition sensor antenna failure or a spacecraft occultation, then communication and relative sensing will not be immediately established. Deployment of spacecraft from the cruise stage can be planned to avoid occultations. In the event of an acquisition sensor antenna failure, the limited-FOV acquisition algorithm of Ref. 8 can be used.

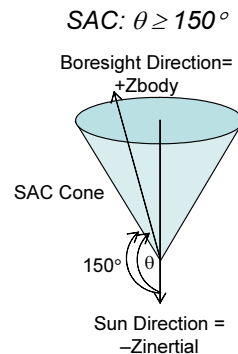


Figure 9. Example Sun Avoidance Constraint.

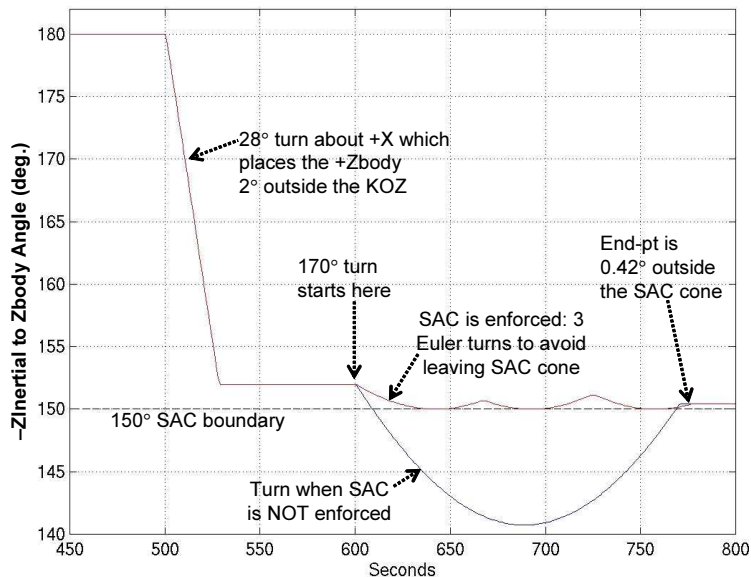


Figure 10. Example of Attitude Replan to Enforce SAC.

Another possibility may be that the spacecraft are out of range of their acquisition sensors. In this case, ground intervention is needed.

For formation reconfiguration, a general deep space, energy-optimal formation reconfiguration algorithm with collision avoidance has been developed.<sup>9</sup> This algorithm does not address the RTC. However, the RTC is not active initially. Therefore, the algorithm of Ref. 9 is used to plan trajectories to move the formation from its post-acquisition configuration to its initial science configuration.

Once the formation has assumed the science configuration and optics have cooled, the RTC is active. Reconfigurations are then needed to retarget the formation between observations. Planning coupled relative translation/attitude reconfigurations with an RTC is an open area of research. Therefore, for retargeting reconfigurations we rotate the formation as a virtual rigid body. This approach satisfies the CAC and RTC, and avoids communication and sensor occultations. Finally, since the initial baseline direction for a new science target is unconstrained, an Euler rotation of the formation, in which the individual spacecraft behave as if embedded in a virtual rigid body, can always be found that satisfies the SAC for the spacecraft.

To illustrate, consider Figure 11. In science configuration, each spacecraft aligns its payload boresight (body z-axis) with the formation boresight  $\vec{s}$ . The collectors must also be aligned along the current baseline vector  $\vec{b}$  with their body x-axes aligned with the baseline. When an initial baseline for Target 2 is specified, an Euler retargeting rotation can cause the aperture boresights to leave their SAC cones. However, when the initial baseline for Target 2 is free, an Euler rotation can always be found that satisfies the SAC during the entire retargeting. If a future mission operational design constrains the initial baseline for a new target, then a sequence of three Euler rotations can be found to satisfy the SAC as in Figure 10. The algorithm for formation rotations is discussed in more detail as part of the observation phase.

We conclude the formation guidance section with formation observations. For observations the formation must be rotated about the formation boresight vector and attitudes must be synchronized with relative positions. For retargeting the formation can be rotated about an arbitrary axis and there is no attitude/relative position synchronization requirement. As a result, the same relative translational guidance algorithm is used for both observation and retargeting rotations. Synchronized attitudes are achieved by commanding each spacecraft to align its body z-axis with the formation boresight and either (i) its body x-axis with the baseline vector or (ii) an assigned body vector with the direction to a neighboring spacecraft.

A formation rotation algorithm has been developed that rotates the formation about the energy-optimal point. The spacecraft travel on a polygonal approximation to arcs, where the number of polygonal segments is commandable. For a two-spacecraft combiner/collector formation, Figure 12 shows a 4-segment 180° formation rotation followed by two 90° rotations of increasing segments. The relative position is shown in a frame attached to the combiner. The combiner does move: it follows an open-loop acceleration profile. In this example, attitudes are synchronized even for rotations that are not about the boresight vector. Figure 13 illustrates this synchronization by showing the angular rate command for the collector in the example.

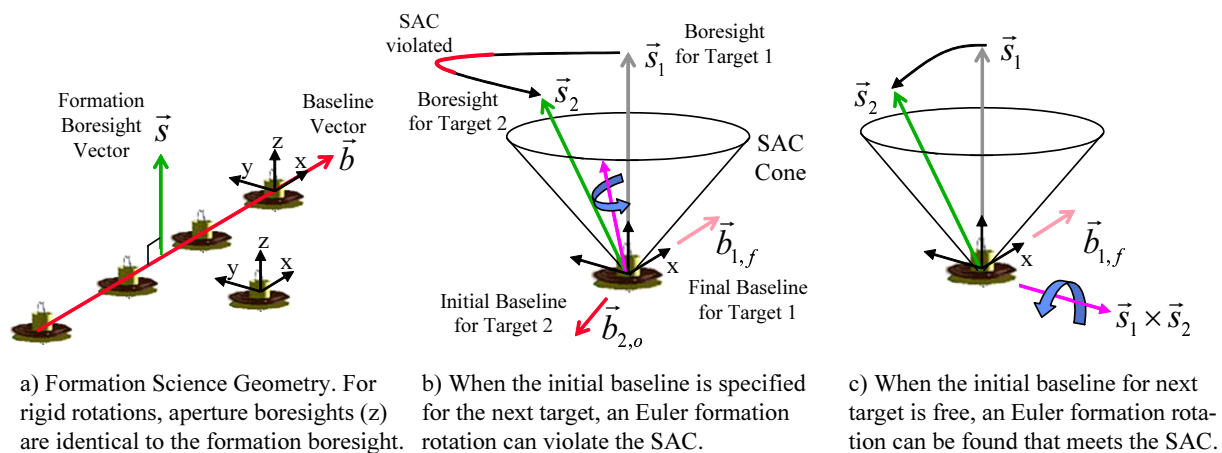


Figure 11. Satisfaction of SAC During Formation Retargeting via Rotation.

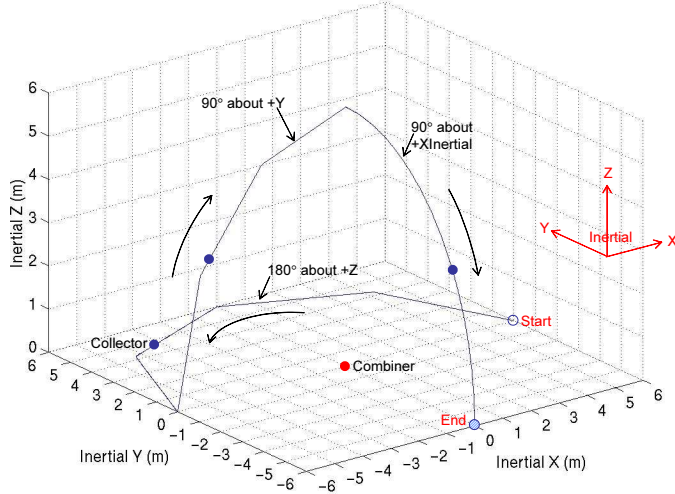


Figure 12. Example Formation Rotation Maneuvers.

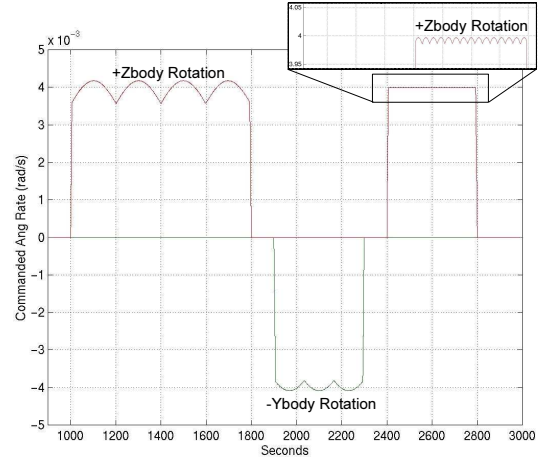


Figure 13. Attitude Synchronization During Rotations.

## VI. Formation and Attitude Control

### A. Control Architecture

The Leader/Follower (L/F) decentralized control architecture was selected for controlling relative spacecraft positions.<sup>10</sup> The L/F architecture is robust (e.g. individual spacecraft failures do not affect the overall stability of the remaining formation), scalable (e.g. spacecraft can be easily added using only local control design), and has deterministic communication requirements. The stability properties of the L/F architecture are also well understood. In particular, for homogenous followers, L/F allows one relative controller to be designed, and this design copied by each follower. For TPF-I, the combiner is the leader, and each collector follows it.

Attitude control (as opposed to guidance) is decoupled from relative translational control. Therefore, independent attitude controllers can be designed. Attitude control is completely decentralized.

In operation, each collector estimates its relative position with respect to the combiner and its inertial attitude. Based on relative translational guidance from the combiner and local attitude guidance, each follower's controllers drive performance errors to within the requirements. The combiner controls its attitude and applies feedforward accelerations as dictated by formation guidance.

There is an important, non-standard constraint on relative position and attitude control. Observations are performed entirely using thrusters. Since the thrusters are not throttleable, their firing can cause spacecraft vibrations that interrupt the interferometer. To allow for both actuation and science, all thrusters on all spacecraft for both attitude and relative position control may only fire in a 6 s window every 54 s. Data gathering occurs during the 54 s between thruster firing windows. This requirement is referred to as the thruster synchronization constraint (TSC).

### B. Formation and Attitude Control Algorithms

For control design, both relative translational and attitude dynamics are well approximated by independent double integrator models. Relative translational control design is simplified since TPF-I will be in orbit about a Sun-Earth Lagrange point. In these orbits, the relative translational dynamics are well approximated by decoupled double integrator models.<sup>11</sup> Similarly, since the TPF-I spacecraft are three-axis stabilized, have small off-diagonal inertias, and rotate slowly, the small angle approximation is valid. In this approximation, the quaternion is decomposed into independent body axis angle errors, and the dynamics of each angle error are approximated by a double integrator model. Since each relative translational and rotational degree of freedom is modelled by a double integrator, one SISO controller can be designed for all degrees of freedom and then scaled to the correct double integrator model (e.g., by multiplying by the inertia about a principal axis).

For control design, we used a classical approach augmented with nonlinear dynamic compensation.<sup>12</sup> The controller is divided into two parts: a fast controller that runs at the 1 Hz FACS rate, and a slow controller that runs at  $1/60^{th}$  of a Hertz. The slow controller output is scaled and applied over 4 s of the 6 s window

with 2 s reserved for margin. Both controllers are stable individually and in parallel. Switching between the fast and slow controllers is done using nonlinearities in the controller, and so no additional mode commander is necessary. The nonlinearities enforce the phase space logic shown in Figure 14. As can be seen, the fast controller turns off when the position tracking error is small. Then actuation only occurs every 60 seconds per the RTC. Also note that there are regions of the phase space where no control is active. The current design is such that the maximum drift time is 17 s. These regions could be removed at the cost of increased controller complexity, but the regions do not affect steady-state tracking performance.

The fast controller is a PD with nonlinear dynamic compensation and includes rate limits in the event of large tracking errors. The slow controller is a PID and also has nonlinear dynamic compensation. The nonlinear compensation in both the fast and slow controllers allows a conditionally stable loop to be designed that is stable in the event of saturations. In effect, high gain controllers have been designed based on the Bode integral constraints that reduce their gain as tracking errors become large.<sup>12</sup>

The control design was simulated to demonstrate its performance. The scenario considered was the control of a collector during an observation with a formation rotation period of 48 hours and the formation plane perpendicular to the Sun-line. Recall that during an observation the spacecraft are travelling on a circle and rotating about their body z-axes to keep their body x-axes aligned with the formation baseline. Therefore, the attitude commands, which are in the body frame, are zero in the body x- and y-axes and a ramp in the body z-axis. Relative translational commands, which are in the inertial frame, are sinusoids in the inertial x- and y-axes, and zero in the inertial z-axis. For convenience, the inertial x-y plane has been chosen to coincide with the formation plane. The full simulation model includes: (i) actuator misalignments of 10 *arcsec*, (ii) estimation noise based on the estimator performance of Section IV, (iii) an extra delay of one RTI, (iv) a sun-shield mode at 0.48 Hz, (v) a solar torque of 0.15 *mNm* about the body x-axis and a differential solar pressure of 0.5 *mN* in the inertial z-axis, (vi) mass and inertia uncertainties of 3%, and (vii) kinematic decoupling errors, which result from realizing inertial force commands with body-fixed thrusters and imperfect attitude knowledge. To ensure performance with margin, the solar-induced disturbances are larger than will be expected in practice.

The steady-state simulation results are given in Figures 15 and 16, which show, respectively, the body x-axis angular tracking error and the inertial x-axis relative translational tracking error. There is a considerable transient (not shown) due to the low bandwidth of the controllers required by the TSC. However, the transient will be reduced when the controllers are integrated with the formation guidance, which provides feedforward accelerations. While we do not explicitly show the thruster firing times, it is apparent that the TSC is met in Figure 15, which shows one-sided deadbanding due to the solar torque every 60 s. Recall that the attitude requirement is 60 *arcsec* and the translational requirement is 6 *mm*. As can be seen from the figures, both requirements are met.

## VII. Conclusions

We have introduced the Formation and Attitude Control System (FACS) being developed as part of the TPF project for demonstrating long-term precision formation performance and robustness. We first discussed the spacecraft dynamic model, which has a fundamental sun-shield mode at approximately 0.5 Hz, the actuators, and the various sensor suites and topologies. Then each element of FACS, estimation, guidance, and control, was discussed in detail. The guidance provided desired relative positions to each of the collectors and desired attitudes during each of the three formation phases. The estimator and controller combined to achieve the 2 *cm* and 1 *arcmin* performance requirements. The controller incorporated the thruster synchronization constraint (TSC) by having a fast and a slow controller. Nonlinear dynamic compensation was used to safely increase controller gain. The estimator, in which relative position estimates are coupled to attitude estimates, includes an acceleration data processing unit to account for low SNR accelerometer measurements and biases. The estimator also drives the inter-spacecraft communication requirements for FACS.

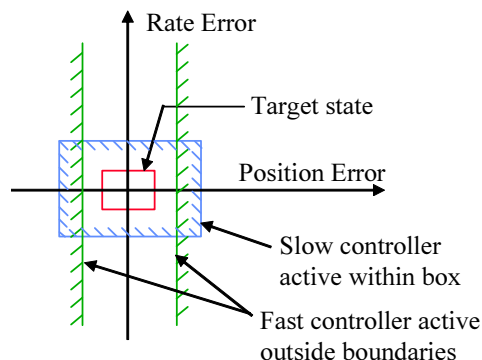
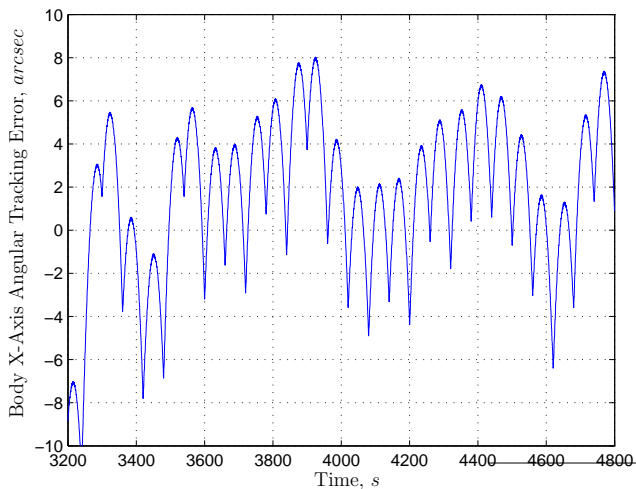
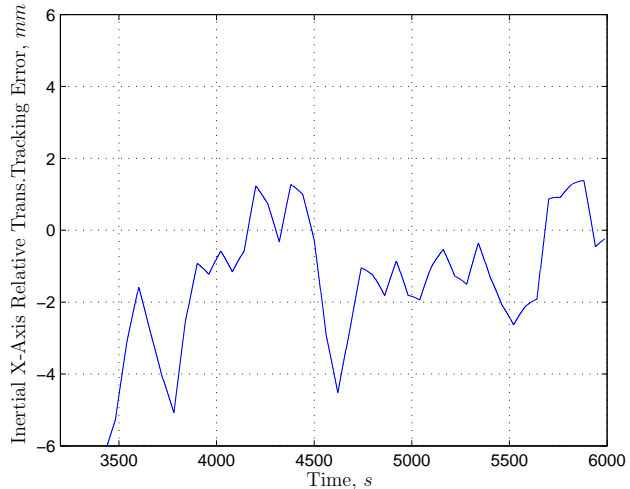


Figure 14. Phase Space Switching between Fast and Slow Controllers.



**Figure 15. Steady-State Attitude Control Performance with TSC.**



**Figure 16. Steady-State Relative Translational Control Performance with TSC.**

The FACS is currently being integrated into the distributed, real-time simulation environment of the Formation Algorithms and Simulation Testbed (FAST). The stand-alone, component simulation results reported in this paper will then be validated in that high-fidelity simulation testbed. Results from these simulations as well as formation fault responses and the formation mode commander, which coordinates the high-level functionality of FACS, will be the subjects of a future paper.

## Acknowledgments

This research was performed at the Jet Propulsion Laboratory, California Institute of Technology, under contract with the National Aeronautics and Space Administration.

## References

- <sup>1</sup>Beichman, C., Woolf, N., and Lindensmith, eds., C., “The Terrestrial Planet Finder (TPF):A NASA Origins Program to Search for Habitable Planets,” JPL Pub. 99-3, Cal. Inst. Tech., Pasadena, CA.
- <sup>2</sup>Lawson, P., “The Terrestrial Planet Finder,” *IEEE Aero. Conf.*, 2001, pp. 2005–2011.
- <sup>3</sup>Fridlund, C., “Darwin—the Infrared Space Interferometry Mission,” *ESA Bulletin*, Vol. 103, 2000, pp. 20–63.
- <sup>4</sup>Lagadec, K., Lebas, J., and Ankersen, F., “GNC System for the Control of the Darwin Free-Flying Interferometer,” *Int. Symp. on Formation Flying Missions & Technologies*, Toulouse, France, 2002.
- <sup>5</sup>Wette, M., Sohl, G., Scharf, D., and Benowitz, E., “The Formation Algorithms and Simulation Testbed,” *Int. Symp. Formation Flying Missions & Technologies*, Washington, D.C., 2004.
- <sup>6</sup>Scharf, D., Hadaegh, F., and Kang, B., “On the Validity of the Double Integrator Approximation in Deep Space Formation Flying,” *Int. Symp. Formation Flying Missions & Technologies*, Toulouse, France, 2002.
- <sup>7</sup>Rasmussen, R., Singh, G., Rathbun, D., and Macala, G., “Behavioral Model Pointing on Cassini Using Target Vectors,” *Annual AAS Guid. & Contr. Conf.*, 1995.
- <sup>8</sup>Scharf, D., Ploen, S., Hadaegh, F., and Sohl, G., “Guaranteed Spatial Initialization of Distributed Spacecraft Formations,” *AIAA Guid., Nav., & Contr. Conf.*, 2004.
- <sup>9</sup>Singh, G. and Hadaegh, F., “Collision Avoidance Guidance for Formation-Flying Applications,” *AIAA Guid., Nav., & Contr. Conf.*, 2001.
- <sup>10</sup>Wang, P. and Hadaegh, F., “Coordination and Control of Multiple Microspacecraft Moving in Formation,” *J. Astro. Sci.*, Vol. 44, No. 3, 1996, pp. 315–355.
- <sup>11</sup>Gómez, G., Lo, M., Masdemont, J., and Museth, K., “Simulation of Formation Flight Near Lagrange Points for the TPF mission,” *AAS/AIAA Astro. Conf.*, 2001.
- <sup>12</sup>Lurie, B., “Multi-mode Synchronized Control for Formation Flying Interferometer,” *AIAA Guid., Nav., & Contr. Conf.*, 2003.